

Excited-eigenstate entanglement properties of XX spin chains with random long-range interactions

Y. Mohdeb^{1,*}, J. Vahedi^{1,2,†} and S. Kettemann^{1,3,‡}

¹*Department of Physics and Earth Sciences, Jacobs University Bremen, Bremen 28759, Germany*

²*Department of Physics, Sari Branch, Islamic Azad University, Sari 48164-194, Iran*

³*Division of Advanced Materials Science, Pohang University of Science and Technology (POSTECH), Pohang 790-784, South Korea*



(Received 8 March 2022; revised 28 July 2022; accepted 8 September 2022; published 14 September 2022)

Quantum information theoretical measures are useful tools for characterizing quantum dynamical phases. However, employing them to study excited states of random spin systems is a challenging problem. Here, we report results for the entanglement entropy (EE) scaling of excited eigenstates of random XX antiferromagnetic spin chains with long-range (LR) interactions decaying as a power law with distance with exponent α . To this end, we extend the real-space renormalization group technique for excited states (RSRG-X) to solve this problem with LR interactions. For comparison, we perform numerical exact diagonalization (ED) calculations. From the distribution of energy-level spacings, as obtained by ED for up to $N \sim 18$ spins, we find indications of a delocalization transition at $\alpha_c \approx 1$ in the middle of the energy spectrum. With RSRG-X and ED, we show that for $\alpha > \alpha^*$ the EE of excited eigenstates retains a logarithmic divergence similar to the one observed for the ground state of the same model, while for $\alpha < \alpha^*$ EE displays an algebraic growth with the subsystem size l , $S_l \sim l^\beta$, with $0 < \beta < 1$. We find that $\alpha^* \approx 1$ coincides with the delocalization transition α_c in the middle of the many-body spectrum. An interpretation of these results based on the structure of the RG rules is proposed, which is due to *rainbow* proliferation for very long-range interactions $\alpha \ll 1$. We also investigate the effective temperature dependence of the EE, allowing us to study the half-chain EE of eigenstates at different energy densities, where we find that the crossover in EE occurs at $\alpha^* < 1$.

DOI: [10.1103/PhysRevB.106.104201](https://doi.org/10.1103/PhysRevB.106.104201)

I. INTRODUCTION

The magnetic properties of doped semiconductors as observed in magnetic resonance experiments [1] motivated P.W. Anderson to address the localization in interacting disordered systems, in particular disordered interacting spin systems [2]. Fleishman and Anderson [3] showed that short-range interactions in an electron system with localized single-particle states might not destroy localization for some range of finite temperature T . In Refs. [4,5], it was argued that many-body localization at finite temperature may result in a lack of thermalization. Since then, many-body localization (MBL) has become a flourishing research direction; for reviews see Refs. [6,7].

In a MBL phase, disorder, as modeled by randomness, can lead to localized states despite the presence of interactions. These states violate the eigenstate thermalization hypothesis (ETH) [8], which states that the statistical properties of physical observables of generic quantum Hamiltonians are the same as those predicted by the microcanonical ensemble. Thereby, given a subregion A of n spins in a chain, ETH requires that entanglement entropy S_A scales with the volume of A , $S_A \sim n$

[6], whereas in a MBL phase, excited eigenstates display an area law entanglement scaling $S_A \sim 1$.

More recently, systems displaying a logarithmic divergence at finite energy density $S_A \sim \ln(n)$, and power law average correlations were discovered [9,10]—they were dubbed *quantum critical glasses*. While, MBL is essentially established for some short-range models [11], random bond spin chains with long-range (LR) interactions have to our knowledge not been investigated, although studies on LR interacting spin chains with random magnetic field have been done [12–14].

As finite temperature MBL is a property associated with excited many-body eigenstates, inspecting their entanglement properties is highly insightful.

To this end, we employ one of the most potent tools for studying one dimensional random Hamiltonians, the strong disorder renormalization group (SDRG) [15,16]. SDRG has been widely used to study properties of ground states of disordered spin chains with nearest-neighbor interactions [17,18] and beyond [19–22] and more recently it was used to describe random spin chains with power-law decaying interactions [23–26]. This method has recently been extended to study the whole set of eigenstates via the so-called RSRG-X (real space renormalization group for excited states) procedure [27]. This technique is a powerful method to characterize the excited states of random interacting many-body systems, and can therefore be used to capture different dynamical phases of a given model at strong disorder. In particular, this procedure

* y.mohdeb@jacobs-university.de

† j.vahedi@jacobs-university.de

‡ s.kettemann@jacobs-university.de

was previously used to study the entanglement properties of excited eigenstates of a random XX spin chain with nearest-neighbor interaction [28,29], where it was found that the flow equations for the magnitude of the couplings are identical to the ground-state ones, therefore leading to a logarithmic divergence in the entanglement entropy (EE). RSRG-X was also used to study the high-energy states of the random bond XXZ spin chain [10].

Here, we consider a random bond-XX spin chain with couplings decaying with a power-law exponent α . Disorder is introduced in the model through a random choice of the positions of the spins on the chain leading to randomness in the spin-spin couplings. We study the excited eigenstate properties of this model via both RSRG-X and numerical exact diagonalization (ED). The ground-state entanglement properties of such a system were previously studied in Ref. [26], where it was found that EE at zero temperature displays a logarithmic enhancement irrespective of the values of α . This was obtained via an analytical formulation of SDRG, its numerical implementation, and using ED.

In the next section, we are using numerical ED to study the level spacing statistics as an indicator for MBL. In Sec. III, RSRG-X is introduced; in Sec. IV, it is applied to derive the EE of this model and its dependence on subsystem size l . In Sec. V, the results for the EE are presented as obtained with ED performed for up to $N \sim 14$ spins. With both methods, we find that in the middle of the many-body spectrum, for any $\alpha > 1$ the EE diverges logarithmically as for conformally invariant systems [30–32] and as observed similarly in the ground state of random spin chains described by a random singlet phase [17,26]. However, for $\alpha < 1$ a subvolume law for entanglement scaling is found $S(l) \sim l^\beta$ with $0 < \beta < 1$, and l being the subsystem size. Thus, we find that the crossover in EE scaling at $\alpha^* \approx 1$ coincides with delocalization transition $\alpha \approx 1$ in the middle of the many body spectrum. In Sec. VI, results for the entanglement contour are presented and analyzed. In Sec. VII, we present an interpretation of the power-law scaling of the EE with subsystem size in terms of rainbow bond proliferation. In Sec. VIII, we present results obtained at finite effective temperature, corresponding to an energy density away from the middle of the spectrum. In Sec. IX, we conclude. Finally, in Appendix A we show ED results for the average correlation functions, while in Appendix B the energy spectrums as obtained via ED and RSRG-X are compared for different values of α .

We focus on the bond disordered XX-spin chain with LR couplings, defined by the Hamiltonian

$$H = \sum_{i < j} J_{ij} (S_i^x S_j^x + S_i^y S_j^y), \quad (1)$$

describing N interacting $S = 1/2$ spins that are placed randomly at positions \mathbf{r}_i on a lattice of length L and lattice spacing a , with density $n = N/L = 1/l_0$, where l_0 is thus the average distance between them. The couplings between all pairs of sites i, j , are taken to be antiferromagnetic and long-ranged, decaying with a power law α :

$$J_{ij} = J_0 |\mathbf{r}_i - \mathbf{r}_j| / a |^{-\alpha}. \quad (2)$$

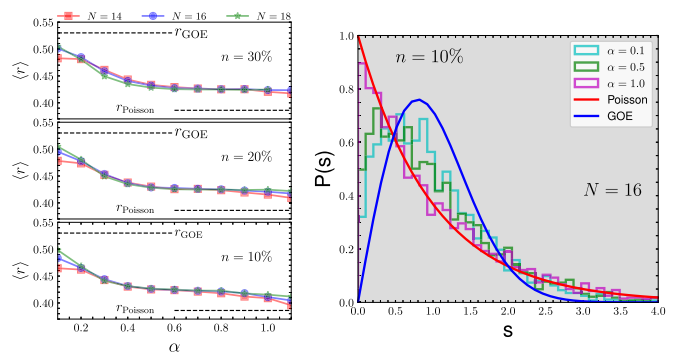


FIG. 1. Left: Adjacent gap ratio for various values of α and filling factors n . Right: Probability distribution $P(s)$ of level spacings $s = E_{n+1} - E_n$ between consecutive unfolded eigenvalues [37]. Note, particularly, that for the probability distribution, we diagonalize the Hamiltonian Eq. (1) in the $S_{\text{tot}} = 0$ - subspaces, as the projection of the total spin along the z axis, $S_{\text{tot}} = \sum_i S_i^z$, is conserved. The results are averaged over 1000 disorder realizations. For the adjacent gap ratio, $N_s = 50$ states are taken in the middle of the many-body spectrum.

We note that for $\alpha = 0$, the above Hamiltonian Eq. (1) corresponds to the isotropic antiferromagnetic Lipkin-Meshkov-Glick model in absence of magnetic field [33]. It is a clean infinite-range model and its ground-state entanglement properties have been investigated in Ref. [34], where it was shown that the EE scales logarithmically with subsystem size.

We fix $J_0 = 1$ and $a = 1$ in the following.

II. LEVEL-SPACING STATISTICS

Level-spacing statistics is known to be a convenient indicator to identify whether a system is in a delocalized phase, a localized phase, or another regime. Disordered Hamiltonians with time-reversal and spin symmetry are known to be described by the Gaussian orthogonal ensemble (GOE), without time-reversal symmetry by the Gaussian unitary ensemble level-spacing statistics, when they are in the ergodic regime as characterised by energy level repulsion. In a localized phase, rather, the level-spacing statistics obeys the Poisson distribution, indicating the absence of level repulsion [35,36]. Via ED, we compute the distribution $P(E_{n+1} - E_n)$ of the energy level spacings of the model Eq. (1) for different filling factors $n = N/L$ and various values of the exponent α . Further, we calculate the ratio of consecutive gaps of distinct energy levels, also known as the adjacent gap ratio,

$$r = \frac{1}{N_s} \sum_n \frac{\min(E_{n+1} - E_n, E_n - E_{n-1})}{\max(E_{n+1} - E_n, E_n - E_{n-1})}, \quad (3)$$

where N_s is the number of states which are taken from the spectrum to calculate r . The value of r , averaged over several disorder realizations, is known to be 0.5307 [35] for the GOE and around 0.386 for the Poisson distribution. Results are shown in Fig. 1, together with both limiting values. Here states are taken from the middle of the many-body spectrum. We see a crossover between a regime where the level spacing approaches the GOE for sufficiently small values of α and a Poisson regime for $\alpha > 1$. In a large interval of $\alpha < 1$,

it is in an intermediate regime. These results suggest the possibility of a delocalization-localization transition occurring at $\alpha_c \approx 1$ in the middle of the many-body spectrum. Note that no qualitative difference is observed for varying densities of spins $n = N/L$. We will therefore fix $n = 0.1$ in the following.

III. RSRG-X METHOD IN THE PRESENCE OF POWER LAW COUPLINGS

Next, we intend to evaluate the EE scaling with subsystem sizes as a function of the exponent α . EE provides a quantitative tool to characterize how information is spread from one part of the system to another. To this end, we use both a renormalization group scheme and numerical ED. We first describe how to apply the RSRG-X to this model with anti-ferromagnetic LR interactions. For the ground state, at each step of SDRG [16,26,38], we identify the largest coupling $J_{ij} = \Omega$ and put the two spins that are coupled by Ω in the lowest energy state, a singlet state. Assuming strong disorder, the coupling of these two spins is much larger than the remaining couplings. We therefore treat them as perturbations and derive an effective Hamiltonian for the remaining spins. This procedure is continued until we form $N/2$ singlet pairs. Thereby, the ground state of the system is approximated as the tensor product of these singlet states within SDRG.

Excited eigenstates can be obtained by a modified version of SDRG, known as RSRG-X. In this method, the two spins with the largest (in magnitude) coupling constant are chosen to be in one of their four eigenstates (one singlet, three triplet states) with energy E by the Boltzmann distribution, depending on an effective temperature T , so for each of the singlet and triplet states, there is a corresponding probability associated with the parameter T . The effective couplings for the other spins then depend on the choice of the state for the two spins. To determine the RG rules for excited states, we make use of degenerate perturbation theory, namely, a Schrieffer-Wolf transformation (SWT) [39] is applied. SWT is a perturbative unitary rotation that eliminates off-diagonal elements of the Hamiltonian H with respect to a *strong* piece H_0 . Specifically, one writes $H = H_0 + V$, where V is parametrically smaller than H_0 , as denoted by $V \in \mathcal{O}(\lambda)$. Then, one searches for a unitary operator e^{iS} such that $[e^{iS}He^{-iS}, H_0] = 0$ to the desired order in V . This results in a self-consistent equation for S at each order, which can then be solved. Further, one projects onto an eigenstate subspace of H_0 , and finds an effective Hamiltonian for the remaining degrees of freedom. Projecting onto the lowest-energy eigenstate at each step of RSRG-X gives the ground state of the model reproducing the usual SDRG scheme, whereas projecting onto other subspaces allows access to generic excited eigenstates.

Here, we give an overview of SWT and derive the RSRG-X rules for the Hamiltonian Eq. (1). We seek for an operator S such that $[e^{iS}He^{-iS}, H_0] = 0$. Expansion of the unitary rotation of H in S gives

$$e^{iS}He^{-iS} = H_0 + V + [iS, (H_0 + V)] - \frac{1}{2}\{S^2, H_0 + V\} + S(H_0 + V)S + \dots, \quad (4)$$

where $\{.,.\}$ stands for the anticommutator. We now expand S in powers of λ , $S = \sum_n S_n$ with $S_n \in \mathcal{O}(\lambda^n)$. The condition

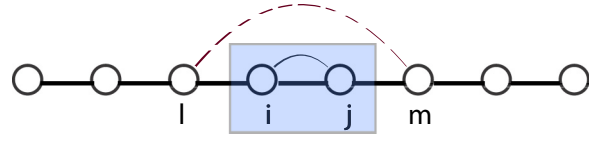


FIG. 2. Decimation of the strongest-coupled pair i, j (highlighted in blue) generates effective couplings between other spins l, m (brown dotted line).

$[e^{iS}He^{-iS}, H_0] = 0$ then fixes the form of S_n . At first order in V , we find

$$S_{(1)} = i \sum_{\alpha \neq \beta} \frac{|\alpha\rangle\langle\alpha|V|\beta\rangle\langle\beta|}{E_\alpha - E_\beta}, \quad (5)$$

where α, β are eigenstates of H_0 , the singlet or one of the triplet states, formed by the spins with the largest coupling, and E_α, E_β are their corresponding eigenvalues. The effective Hamiltonian is then given by the first order expansion in V of Eq. (4), namely,

$$H_{\text{eff}} = e^{iS_1}He^{-iS_1} - H_0 = \sum_{\alpha} |\alpha\rangle\langle\alpha|(V + [iS_1, V])|\alpha\rangle\langle\alpha|. \quad (6)$$

Having described the framework for performing our degenerate perturbation theory, we now apply this procedure to the Hamiltonian in Eq. (1). In the case of the LR spin chain, one obtains the first-order effective Hamiltonian and therefore deduces the RG rules for the different choices of projections for H_0 . Crucially, we note that the effective Hamiltonian keeps the XX form of the original one, as the effective spins created along RSRG-X flow completely decouple from the rest of the chain. This allows the procedure to be readily iterated. The results are summarized below. Here, (i, j) denotes the pair with the strongest coupling, as shown in Fig. 2. If the pair (i, j) is projected onto $|\uparrow\uparrow\rangle$ or $|\downarrow\downarrow\rangle$, we obtain

$$(J_{lm})' = J_{lm} - \frac{J_{il}J_{jm} + J_{im}J_{jl}}{J_{ij}}. \quad (7)$$

If (i, j) is in $(|\uparrow\downarrow\rangle + |\downarrow\uparrow\rangle)/\sqrt{2}$:

$$(J_{lm})' = J_{lm} + \frac{(J_{li} + J_{lj})(J_{im} + J_{jm})}{J_{ij}}. \quad (8)$$

If (i, j) is in $(|\uparrow\downarrow\rangle - |\downarrow\uparrow\rangle)/\sqrt{2}$, we recover the result of Refs. [24,26]:

$$(J_{lm})' = J_{lm} - \frac{(J_{li} - J_{lj})(J_{im} - J_{jm})}{J_{ij}}. \quad (9)$$

The RSRG-X procedure consists of reiterating this scheme and updating the value of all couplings at each RG step. Thereby, a generic RSRG-X eigenstate is obtained by taking the tensor product of all singlet and triplet pairs obtained along the RSRG-X flow. We note that, due to the RG rule in Eq. (7), the generation of ferromagnetic couplings along the RG flow is possible. This is also the case for the RSRG-X applied to the nearest-neighbor XX spin chain [28]. In the case of a ferromagnetic coupling, the high-energy projection becomes the singlet state.

IV. ENTANGLEMENT ENTROPY

The EE of a pure state ρ_{AB} is defined as

$$S(\rho_A) = -\text{Tr}(\rho_A \ln(\rho_A)), \quad (10)$$

where $\rho_A = \text{Tr}_B(|\psi\rangle\langle\psi|)$ is the reduced density matrix after tracing out a part B of the system and $|\psi\rangle$ is the considered eigenstate. It is an important diagnostic to identify phase transitions in disordered quantum systems [9,12].

We aim to evaluate the thermally averaged entanglement entropy of a part A of length l of a spin chain, $\langle S_T(l) \rangle$ with eigenstates $|\psi_i\rangle$ sampled from the Boltzmann distribution at effective temperature T [28],

$$\langle S_T(l) \rangle = \left\langle \sum_i \frac{\exp(-\frac{1}{T}\langle\psi_i|H|\psi_i\rangle) S(l)|\psi_i\rangle}{Z(T)} \right\rangle, \quad (11)$$

where $\langle \cdot \rangle$ stands for the disorder average and $S(l)|\psi_i\rangle$ is the EE Eq. (10) with subsystem length l , when the system is divided into two subsystems of sizes l and $L-l$, respectively, in state $|\psi_i\rangle$ with density matrix $\rho_i = |\psi_i\rangle\langle\psi_i|$.

To obtain this EE, we use the fact that if the spins i and j are projected onto a singlet state or to the entangled triplet state $(|\uparrow\downarrow\rangle + |\downarrow\uparrow\rangle)/\sqrt{2}$, a unit $\ln 2$ of entanglement is generated, whereas the two other triplet states $|\uparrow\uparrow\rangle$ and $|\downarrow\downarrow\rangle$ are not entangled and thus do not contribute to the EE.

At a given parameter T , we then sample the states from the Boltzmann distribution for every disorder realization by choosing at each step of the RSRG-X procedure to project the most strongly coupled pair of spins to a singlet or one of the triplet states, chosen according to the respective largest probability determined by their energy E and parameter T . For each disorder realization, we then take the average of the thus generated EE for all eigenstates $|\psi_i\rangle$ at fixed T . Note that $\langle S_T(T) \rangle$ is not the EE of the thermally mixed states but rather the EE of pure eigenstates sampled around a certain energy region as determined by the effective temperature parameter T .

In Fig. 3, we show the results in the limit of infinite effective temperature $T \rightarrow \infty$, where all eigenstates are sampled equiprobably in the middle of the energy spectrum [9]. The average EE of eigenstates as a function of the partition length l (physical distance) is displayed for different values of α for $N = 200$ spins, here we have considered the average over $N_s = 100$ states in the middle of the many-body spectrum. We have checked that the results are similar for different values of N_s .

A clear increase of EE is observed as α is lowered for $\alpha < 1$, while the results for $\alpha = 1.8$ and $\alpha = 2.8$ are almost identical.

For $\alpha < 1$, the EE grows with l slower than volume law, which would be linear in l . We observe in Fig. 4 (top) that on a log-log scale, the EE for each $\alpha < 1$ can be fitted with a straight line, $\ln(S_l) = \beta \ln(l) + a$. Thus, the EE obeys a power-law dependence on partition length, $S_l = al^\beta$, with fitted power smaller than one, $\beta < 1$, for all $\alpha < 1$. Such a power-law behavior is due to the presence of sufficiently LR interactions in this model, and was previously observed for the ground states of the power-law random banded model [40] as reported in Ref. [41], but also for the ground states

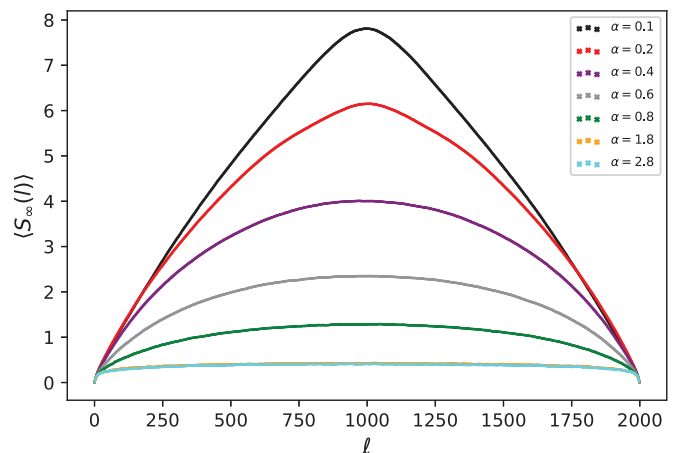


FIG. 3. Average entanglement entropy of excited eigenstates at infinite effective temperature as a function of the partition length l (physical distance), obtained from numerical RSRG-X for the long-ranged XX-chain with open boundary conditions for $N = 200$ spins for various values of α . The filling factor was fixed to $N/L = 0.1$. The average was evaluated over 10 000 disorder realizations, and $N_s = 100$ sampled states for each disorder realization.

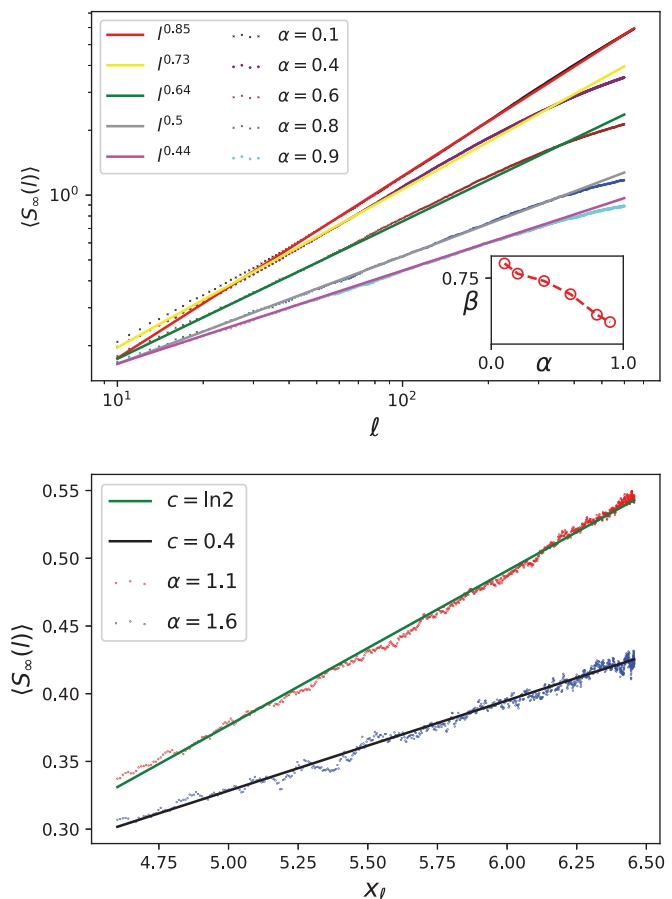


FIG. 4. Top: Fig. 3 on log-log scale for $\alpha < 1$, the inset plot shows β the exponent in $S \sim l^\beta$ as a function of α . Bottom: EE as a function of the logarithm of the chord distance x_l for $\alpha = 1.1$ and $\alpha = 1.6$. Here, c stands for the effective central charges. Results are obtained from numerical RSRG-X for $N = 200$ spins at filling factor was fixed to $N/L = 0.1$, averaged over 10 000 disorder realizations, for $N_s = 100$ sampled states for each disorder realization.

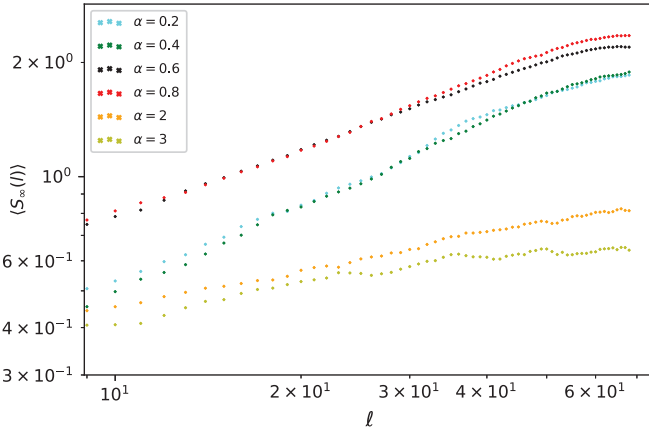


FIG. 5. ED average entanglement entropy in the middle of the energy spectrum for $N = 14$ spins and a filling factor $N/L = 0.1$ for various values of α . The results are obtained for 250 realizations, averaging over $N_s = 20$ states for each disorder point.

of free fermions with LR hoppings and XX spin chains with LR couplings of random sign and amplitude [42,43].

For $\alpha > 1$, the EE displays a logarithmic enhancement. A similar behavior was observed in the nearest-neighbor XX random spin chain [28], where it was found that the average EE of a subsystem of size n scales as $S(n) = (c_{\text{eff}}/6) \ln(n)$ with $c_{\text{eff}} = a \ln 2$ and where $1/2 \leq a \leq 1$ is an undetermined prefactor due to degeneracy.

To confirm this, we plot the average EE for $\alpha = 1.1$ and $\alpha = 1.6$ in Fig. 4 (bottom) as a function of the logarithm of the chord distance, $x_l = \ln(\frac{L}{\pi} \sin(\frac{\pi l}{L}))$. Indeed, the EE turns out to be linear on this scale with a slope $a = \frac{c_{\text{eff}}}{6}$ corresponding to a logarithmic law for open boundary conditions [30,31], with an effective central charge $c_{\text{eff}} = \ln 2$ for $\alpha = 1.1$ and $c_{\text{eff}} = 0.4$ for $\alpha = 1.6$, as plotted as dashed lines.

The exponent of the power-law EE divergence, β , is found to decrease with increasing α for $0 < \alpha < 1$ as can be seen in the inset plot of Fig. 4. For $\alpha > 1$, the EE scaling turns into a logarithmic dependence on l for any $\alpha > 1$, as shown exemplarily in Fig. 4 (bottom) for $\alpha = 1.1$ and $\alpha = 1.6$. We mention that the results are presented here for the EE as a function of the real distance $l = r_i - r_j$, where r_i is the position of spin i , to be contrasted with the index distances $n = |i - j|$ between the spins. Similar scaling is observed as a function of the index distances.

V. ED STUDY OF ENTANGLEMENT ENTROPY SCALING

Although limited to small system sizes, numerical ED has been extensively used to study the properties of excited states of random and disordered spin chains [12,35,36,44,45]. We perform numerical ED on the Hamiltonian in Eq. (1). Average EE is then evaluated for $L = 140$ sites, a filling factor $\frac{N}{L} = 0.1$, and open boundary conditions for various values of α in the middle of the energy spectrum. Figure 5 shows the average EE in the center of the energy spectrum or (equivalently for $T \rightarrow \infty$) for α ranging between 0.2 and 3. The average EE in the middle of the energy spectrum displays a power-law divergence for $\alpha < 1$, $S(l) \sim l^\beta$ with $0 < \beta < 1$, as can be

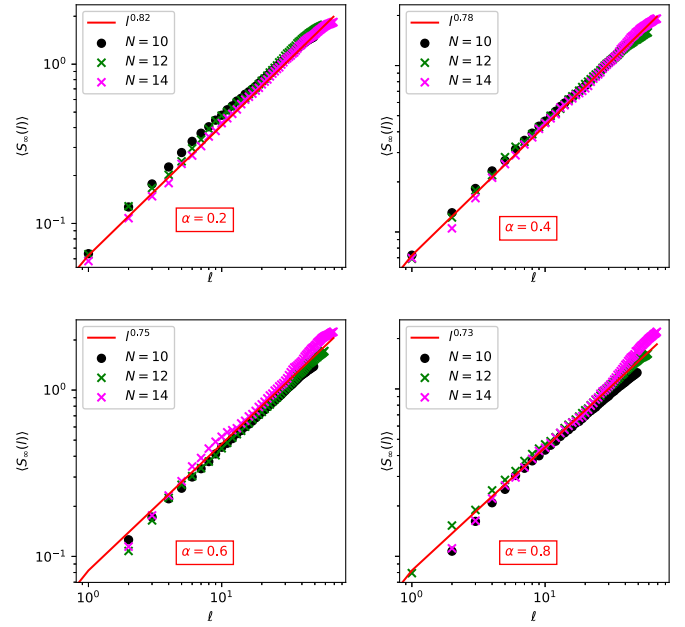


FIG. 6. EE on log-log scale for $\alpha < 1$ as obtained by numerical ED for $N = 10, 12, 14$, a filling factor $n = 0.1$, and different values of α . Results are shown for $N_s = 50$ states in the middle of the many-body spectrum and for 500 disorder realizations. The red curves are functions of the form al^β with fitted β as indicated.

observed in Fig. 6, in agreement with the results obtained by RSRG-X, reported in the previous section. For $\alpha > 1$, the EE scaling shows a logarithmic enhancement similar to what was found for the ground state, in agreement with RSRG-X. The entanglement scaling exponents β obtained by fitting the ED data are in good agreement with what was found through the RSRG-X procedure as can be seen in Fig. 7, where the values of the exponent β are shown for different system sizes. As N is increased for fixed α , the exponent β converges to a value close to the one obtained via ED. Clearly, the convergence is slower for larger α . This can be explained by the smaller perturbative corrections in this case, which imply a larger RG-time to reach the fixed point.

VI. ENTANGLEMENT CONTOUR

A related interesting quantity is the contour for the EE [46,47]. In a lattice, where a spatial cut separating the chain

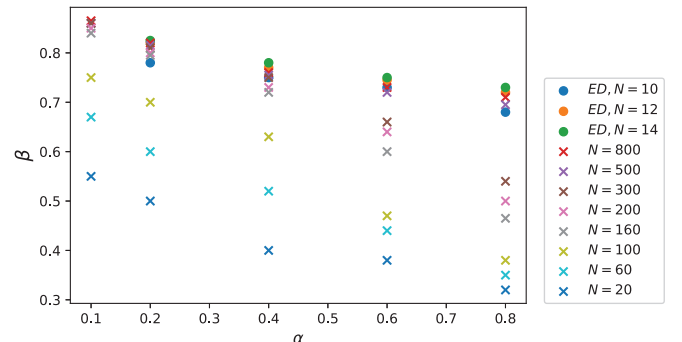


FIG. 7. The exponent β as function of $\alpha < 1$, as obtained by fitting the ED and RSRG-X results to the function $S(l) \sim l^\beta$.

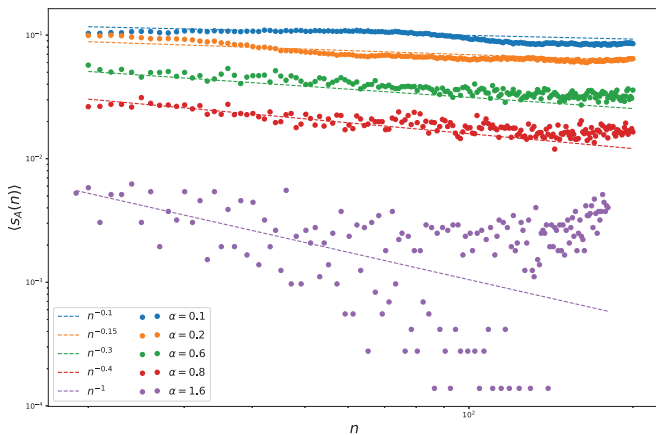


FIG. 8. Entanglement contour as obtained via RSRG-X at infinite effective temperature for the LR random XX chain for different values of α . Data points were obtained for $N = 500$ spins randomly placed among $L = 5000$ sites. The figure shows the entanglement contour $s_A(n)$ as a function of position n inside block A of the chain. Here block A was chosen to be the left half of the chain containing $N/2$ spins. Each data point was obtained by averaging over 2000 disorder realizations and 50 sampled states at each disorder realization.

in two subsystems A and B has been introduced, it is given by a function $s_A(i)$ which provides information about the contribution of the i th site in A to the entanglement between A and B . By construction, the minimal properties that the contour function must satisfy are

$$S_A = \sum_{i \in A} s_A(i), \quad s_A(i) > 0, \quad (12)$$

where the first condition in Eq. (12) is a normalization, while the second ensures that the contribution of each site to the EE is positive.

Within the RSRG-X framework for excited states of random spin chains, a natural definition of the entanglement contour arises, namely, the value of $s_A(i)$ on a given site i in A is given by $\ln 2$ if there is a bond starting at site i and ending in B and if this link is a singlet or an entangled triplet, while $s_A(i)$ is zero otherwise.

Results for the contour function $s_A(n)$ in the LR random XX chain as a function of the position index n in A , as obtained via RSRG-X at infinite effective temperature, $T \rightarrow \infty$ are displayed in Fig. 8 for different values of α . Here, we have taken block A to be the left half of the chain that contains $N/2$ spins. n is the index distance measured from the center of the chain. The figure shows $\langle s_{N/2}(n) \rangle$, that is the average contribution of the n th spin to the EE between the left half and right half of the chain.

From Fig. 8, we see that a strong α dependence appears. Indeed, for $\alpha < 1$, $s_{N/2} \sim n^{-\gamma}$ with $0 < \gamma < 1$. While for $\alpha > 1$ we obtain that $s_{N/2} \sim n^{-1}$. Since the EE of a subsystem of n spins is given by $S_n = \sum_{i=1}^n s_A(i)$, we find, in the limit of $N \gg 1$, that for $\alpha > 1$ the EE diverges logarithmically $S_n \sim \ln(n)$, as it was obtained above via ED and RSRG-X. Whereas for $\alpha < 1$, this yields a power-law growth of EE as a leading term, $S_n \sim n^{1-\gamma}$. This result is consistent with $S_n \sim n^\beta$ previously found using RSRG-X and ED for $\alpha < 1$,

since $\beta \sim 1 - \gamma$. Strikingly, we note that for $\alpha \ll 1$, the entanglement contour exponent γ approaches the bare coupling exponent α . Although we do not have an analytic understanding of this behavior, we conjecture that $\gamma \sim \alpha$ for $\alpha \ll 1$.

VII. TOWARD A SCALING THEORY OF THE POWER LAW ENTANGLEMENT ENTROPY

In the previous sections, we found a strong violation of the area law, an anomalous scaling law for the average EE given by $S_l \sim l^\beta$, with $\beta(\alpha) < 1$ a decreasing function of α for $\alpha < 1$ both with the ED and with the RSRG-X method. Both methods yield good quantitative agreement for $\beta(\alpha)$ as shown in Fig. 7. Still, it is desirable to get an intuitive understanding why the scaling has this anomalous behavior for $\alpha < 1$. To this end, we aim to formulate an entanglement scaling theory in this section.

In Ref. [48], a SDRG procedure was used to study the ground-state entanglement properties of XX spin chains with particular local inhomogeneities. There, the couplings were defined such that RG produces for the ground state a product of concentric singlets, resembling *rainbows*, resulting in a volume law scaling of the EE. This is now known as the rainbow chain [49,50]. More recently, disorder was introduced in such a model, resulting in a coexistence of rainbows and dimer bonds of neighbored spins for the ground state and giving rise to a weaker area law violation [51] in form of a power-law $S_l \sim l^{0.5}$. This motivates us to use ideas developed in these papers, and adapt them to the RSRG-X scheme to understand the peculiar algebraic scaling and its dependence on α of EE in presence of LR interactions.

Let us start from the set of RSRG-X rules Eqs. (8)–(9), which we derived for the Hamiltonian Eq. (1) to qualitatively derive the EE scaling with subsystem size l . First, note that the perturbative corrections for the triplet states Eq. (8) and (7) are typically larger than the ones for singlet states, Eq. (9). This is especially true for small values of $\alpha \ll 1$, resulting in larger renormalized values of the couplings J_{ij} . For $\alpha \gg 1$, the perturbative corrections are significantly smaller, thereby the couplings distribution flows to a strong disorder fixed point as was previously observed for the ground state of the same model [26].

We show now that the RG rule for the *entangled triplet state* Eq. (8) favors the formation of rainbows. Here, a rainbow is defined to be any pair of spins with a bond which is not connecting neighboring sites and is thus not a dimer (bond connecting neighboring sites). To illustrate this, assume that a pair $(n, n+1)$ is projected onto the entangled triplet state $(|\uparrow\uparrow\rangle + |\downarrow\downarrow\rangle)/\sqrt{2}$. Then, based on the observation that the perturbative corrections are typically smaller for sites farther from the decimated bond, the coupling $J_{n-1, n+2}$ is likely to take the largest correction. This leads to the fact that the next decimated bond would be between the sites $(n-1, n+2)$.

The RG rule for the nonentangled triplet states Eq. (7) also tends to create rainbows. Indeed, when a pair $(n, n+1)$ is projected onto the states $|\uparrow\uparrow\rangle$ or $|\downarrow\downarrow\rangle$, the coupling $J_{n-1, n+2}$ is likely to take the largest (in magnitude) correction. The perturbative corrections due to projections onto the nonentangled triplets often induce a change of signs in all the active couplings, therefore leading to the decimation

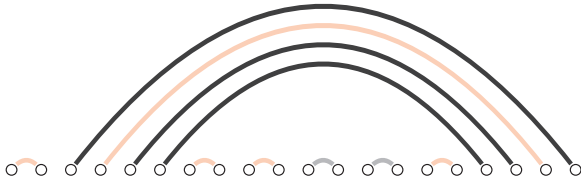


FIG. 9. Illustration of a realization at $N = 20$. The orange bonds represent pairs projected onto $|\uparrow\uparrow\rangle$ or $|\downarrow\downarrow\rangle$, while black links stand for $(|\uparrow\downarrow\rangle + |\downarrow\uparrow\rangle)/\sqrt{2}$ and the grey ones are singlets.

of the pair $(n - 1, n + 2)$ in the next RG step, regardless of the sign of the couplings. Thereby, the nonentangled triplet RG rule produces rainbows similar to the entangled triplet described above, while, as for the ground state, the singlet state projection tends to create more dimers. Thus, the RG rules lead to a state of consecutive dimers which are spanned over by rainbows (bonds connecting farther sites). This picture is expected to become more accurate with smaller α , since the renormalization corrections increase with smaller α , thereby favoring more frequent rainbow formation.

To evaluate the entanglement scaling with subsystem sizes, we define m_d as the number of consecutive dimers regardless of the state they are projected onto. A configuration for $N = 20$ is shown in Fig. 9. In this configuration, there are two dimer regions. The first one is made of one bond $m_d = 1$ (the bond connecting the sites $n = 1$ and $n = 2$), while the other dimer region is composed of five bonds (from spin at site $n = 7$ to $n = 16$), so $m_d = 5$. While there is one rainbow region with $m_r = 4$. Different colors indicate to which state the pair is projected to.

The EE is due to rainbow links which are ranging across the boundary of the subsystem and which are projected either onto the singlet state or the entangled triplet state (in the large system limit we may disregard the entanglement from a single dimer which may cross the boundary). We assume that the rainbows are connecting sites symmetric around the middle of the chain, and are therefore links connecting sites $i, N - i$, as can be qualitatively observed in Fig. 10 (top), for sufficiently small α .

Let the spins in a subsystem be numbered from 1 to n with $n < N/2$ and consider site i and its bond. As dimers do not contribute to the EE, one can write

$$\langle S_n \rangle \sim \frac{1}{2} \ln 2 \sum_{i=1}^n P(i^{\text{th}} \text{ bond is a rainbow}), \quad (13)$$

where the factor $1/2$ is due to the fact that only two states out of the four possible contribute to EE, and $\ln 2$ is the amount of entanglement generated by a singlet or an entangled triplet. Note that here we use n as the index distance. Assuming that the distribution of rainbows along the chain is homogeneous:

$$\langle S_n \rangle \sim \frac{1}{2} (\ln 2) n P(\text{ith bond is a rainbow}). \quad (14)$$

Thereby, as a link belongs either to a rainbow region or to a dimer region, $P(\text{a link is a rainbow}) \sim \frac{n_r}{n_r + n_d}$, where n_r is the number of rainbow bonds and $n_r + n_d$ is the total number of bonds within a subsystem of n spins. If we further assume that the rainbow (and the dimer) regions are homogeneously distributed, $n_r = \langle m_r \rangle N_r$ rainbow bonds and $n_d = \langle m_d \rangle N_r$, where

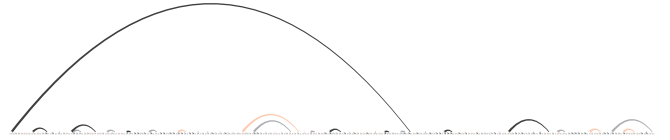
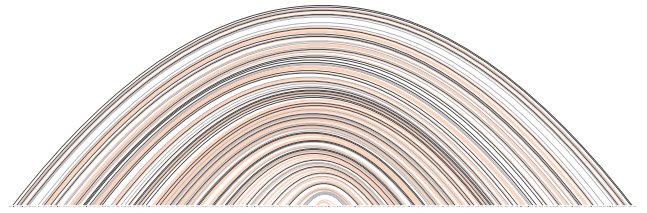


FIG. 10. Top: Typical eigenstate produced by RSRG-X for $\alpha = 0.1$ obtained for $N = 400$ spins and a filling factor $\frac{N}{L} = 0.1$. The bonds in black are pairs projected onto $\frac{1}{\sqrt{2}}(|\uparrow\downarrow\rangle + |\downarrow\uparrow\rangle)$ while the orange links are in the states $|\uparrow\uparrow\rangle$ or $|\downarrow\downarrow\rangle$, and the grey ones are singlets. Bottom: Same but for $\alpha = 1.6$.

N_r is the number of rainbow (dimer) regions. We thus obtain that the EE of a subsystem of n spins can be approximated as

$$\langle S_n \rangle \sim \frac{1}{2} (\ln 2) n \frac{\langle m_r \rangle}{\langle m_r \rangle + \langle m_d \rangle}. \quad (15)$$

In the case of the rainbow chain [48], one has $\langle m_r \rangle = n$ and $\langle m_d \rangle = 1$, yielding a volume-law entanglement $S_n \sim n$. Thus, it remains to evaluate $\langle m_d \rangle$ and $\langle m_r \rangle$.

Let us first derive $\text{Pr}(m_r = k)$, the probability mass function (PMF) of the rainbow region length. We assume that rainbow regions are formed successively along the RSRG-X flow. Since a newly formed bond can only be a rainbow or a dimer, and the three possible triplet projections favor rainbow region expansion, the probability that a region is formed of k rainbows is equal to the probability of forming successively k rainbows with probability $3/4$ for each, then forming a dimer with probability $1/4$. The PMF $\text{Pr}(m_r = k)$ can thus be approximated by a geometric distribution, with $p = 1/4$, yielding $\text{Pr}(m_r = k) = (3/4)^k (1/4)$.

Figure 11 (top) shows the decay of $P(m_r)$ for $\alpha = 0.1$ and $\alpha = 0.2$ as obtained via RSRG-X at infinite effective temperature. Here, a logarithmic scale was used for the ity axis. Clearly, the geometric distribution with $p = 1/4$ provides a good approximation for $P(m_r)$ for both $\alpha = 0.1$ and $\alpha = 0.2$. Thus, as $P(m_r)$ decays very quickly (exponential decay in the continuum limit) $\langle m_r \rangle = \sum_{k=0}^{n/2} k P(m_r = k)$ is a constant not dependent on n for sufficiently large n .

Moreover, $\langle m_d \rangle$ can be directly related to the entanglement contour $s_{N/2}(n)$. Indeed, as the dimer bonds do not contribute to EE, $s_{N/2}(n)$ is the probability that the link starting at the n th spin is a rainbow, which was obtained above under the homogeneity assumption $s_{N/2}(n) \sim \frac{\langle m_r \rangle}{\langle m_r \rangle + \langle m_d \rangle}$. As $\langle m_r \rangle \sim 1$, and since for $\alpha \ll 1$, $s_{N/2}(n) \sim n^{-\alpha}$, we obtain that for $\alpha = 0.1$, $\langle m_d \rangle \sim \frac{1}{s_{N/2}(n)} \sim n^{0.1}$, while for $\alpha = 0.2$, this implies $\langle m_d \rangle \sim n^{0.2}$. Note that for the rainbow chain this yields $s_{N/2}(n) \sim \frac{\langle m_r \rangle}{\langle m_r \rangle + \langle m_d \rangle} \sim 1$ which is consistent since all the sites equally contribute to EE.

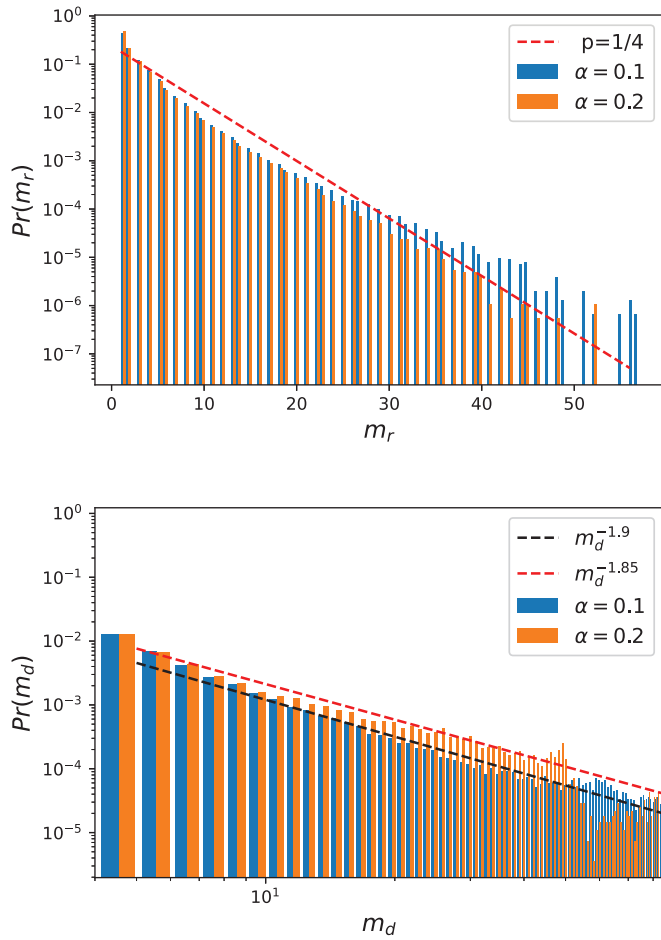


FIG. 11. Top: Probability distribution of the lengths of the rainbow regions $P(m_r)$ for $\alpha = 0.2$ and $\alpha = 0.1$. The red dashed line is a geometric distribution with $p = 1/4$. Bottom: Probability distribution of the length of the dimer regions $P(m_d)$. The histograms were obtained for 30 000 realizations, $N = 300$ and a filling factor $\frac{N}{L} = 0.1$.

To confirm this result, we implement the RSRG-X procedure at infinite effective temperature and numerically compute the histograms of the lengths of dimer regions for sufficiently small values of α . Results are shown in Fig. 11 for $\alpha = 0.1$ and $\alpha = 0.2$. From Fig. 11 (bottom), we obtain that $P(m_d) \sim m_d^{-1.9}$ for $\alpha = 0.1$, leading to $\langle m_d \rangle = \sum_{k=1}^n kP(m_d = k) \sim n^{0.1}$, as obtained using the entanglement contour, therefore

$$\langle S_n \rangle \sim \frac{n}{\langle m_d \rangle} \sim n^{0.9}. \quad (16)$$

Similarly Fig. 11 indicates that for $\alpha = 0.2$, $P(m_d) \sim m_d^{-1.85}$, which thereby leads to $\langle S_n \rangle \sim n^{0.85}$. The power exponents β obtained through this description therefore turn out to be in good agreement with those we have obtained for $\alpha \ll 1$, as can be seen in Fig. 7.

We emphasize that this picture is expected to break down for higher values of α , $0.4 < \alpha < 1$ as the corrections to the couplings are less significant, leading to a less probable rainbow formation, and therefore lower entanglement, whereas for $\alpha > 1$ the perturbative corrections are small enough to flow to a strong disorder fixed point of random bonds (similar

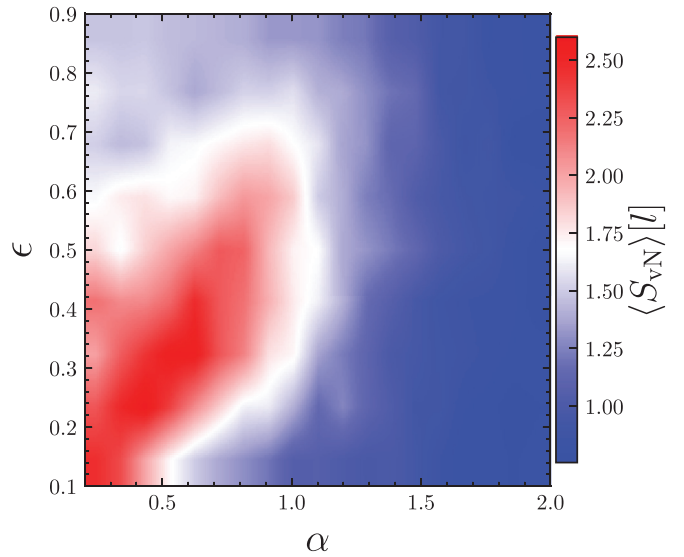


FIG. 12. Half-chain entanglement entropy $S_{l/2}$ for different values of α and at different energy scales ϵ . The results are obtained for $N = 18$, a filling factor $\frac{N}{L} = 0.1$, and $M = 1000$ disorder realizations.

to the ground state, which is a random singlet state). Since each bond may be with probability $1/2$ an entangled state, this explains the logarithmic enhancement of EE. Figure 10 shows two typical eigenstate structures as obtained by RSRG-X for $N = 400$ spins, for a small value $\alpha = 0.1$ and a higher value $\alpha = 1.6$. For $\alpha = 0.1$, we clearly observe a proliferation of rainbow bonds, inducing links connecting farther sites in the chain, and therefore generating stronger entanglement $S_n \sim n^{0.9}$, while for $\alpha = 1.6$ dimer bonds are dominant, and spins which are paired with far away spins are very rare, similar to the $T = 0$ random singlet phase, yielding a logarithmic enhancement of EE.

VIII. ENERGY AND EFFECTIVE TEMPERATURE DEPENDENCE OF ENTANGLEMENT ENTROPY

As we have so far only considered the model in the middle of the many-body spectrum, we now explore the half-chain EE $S_\epsilon(L/2)$ of the eigenstates at different energy densities, aiming to evaluate how the entanglement depends on the energy scale.

A. Energy dependence

First, we employ exact numerical diagonalization: We sample 50 states close to a target energy ϵ for every disorder realization and then calculate the average EE in the middle of the chain $l = L/2$. The energies ϵ are normalized to be in the interval $[0, 1]$ as $\epsilon = (E - E_{\min}) / (E_{\max} - E_{\min})$, where E_{\min} is the ground-state energy. Results for $\epsilon \in [0.1, 0.9]$, $N = 18$ spins and $L = 180$ are shown in Fig. 12. First, we note that around the middle of the energy spectrum $\epsilon \in [0.3, 0.6]$, a crossover between a regime with higher entanglement and a less entangled phase occurs at $\alpha^* \approx 1$, confirming the previously obtained results via both ED and RSRG-X. However, for smaller energies, we observe that there is a shift toward smaller values of α^* , namely, for $\epsilon \in [0.1, 0.3]$ we see that

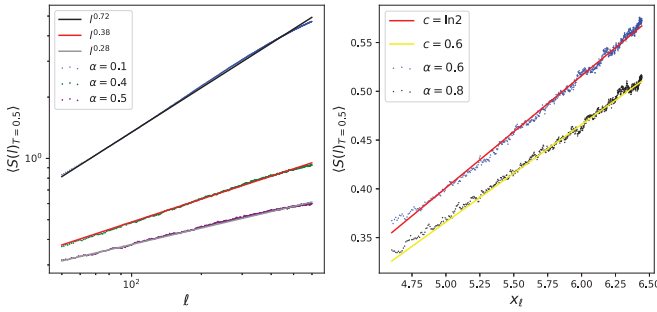


FIG. 13. Average entanglement entropy of excited eigenstates at finite effective temperature $T = 0.5$ as a function of the partition length l (physical distance) and the logarithmic chord distance x_l as obtained via RSRG-X for $N = 200$ spins. The filling factor $\frac{N}{L} = 0.1$ was considered for various values of α . The average was evaluated over 5000 disorder realizations, and 100 sampled states for each disorder realization.

α^* ranges between 0.6 and 0.8, while the crossover is not observed in the half-chain EE at very high energies.

B. Effective temperature dependence

Next, let us implement RSRG-X to explore the effective temperature dependence of EE. To this end, we employ RSRG-X as described in Sec. III, but this time at finite effective temperature parameter T . We fix $T = 0.5$ and sample 100 eigenstates for each disorder realization via the RSRG-X procedure, then calculate the resulting EE as a function of subsystem sizes l for different values of α . Results are shown in Fig. 13. For $\alpha < 0.6$, we observe a power-law growth of EE $S_l \sim l^\beta$ as a function of the partition length. The exponents β are, however, lowered as compared to the $T \sim \infty$ case, as can be seen in Fig. 13 (left) where average EE is plotted against subsystem sizes, and turns out to be linear on the log-log scale, while, for $\alpha \geq 0.6$, EE displays a logarithmic enhancement as can be seen in Fig. 13 (right) where EE is plotted as function of the logarithm of the chord distance $x_l = \ln(\frac{l}{\pi} \sin(\frac{\pi l}{L}))$ for $\alpha = 0.6$ and $\alpha = 0.8$ resulting in a logarithmic enhancement with central charges $c_{\text{eff}} = \ln 2$ and $c_{\text{eff}} = 0.6$, respectively.

These results indicate that at lower effective temperature, the highly entangled phase survives only up to $\alpha^* \approx 0.6$. This can be explained by the rarefaction of projections onto $(|\uparrow\downarrow\rangle + |\downarrow\uparrow\rangle)/\sqrt{2}$ for smaller effective temperatures, therefore inducing a less prevalent rainbow formation and thus a smaller EE for a given α .

IX. CONCLUSION

We introduced a real-space renormalization group scheme for excited eigenstates, a modified RSRG-X, for XX spin chains with random interactions decaying as a power law with distance. The EE is calculated using RSRG-X and ED for different values of the power exponent α in the middle of the many-body spectrum. The results obtained via RSRG-X and ED are in good agreement and show that the average excited eigenstate EE grows as a power law with the subsystem size l , $S(l) \sim l^\beta$, with power $0 < \beta < 1$ a decreasing function of α for $\alpha < \alpha^*$, while a logarithmic enhancement of EE entropy

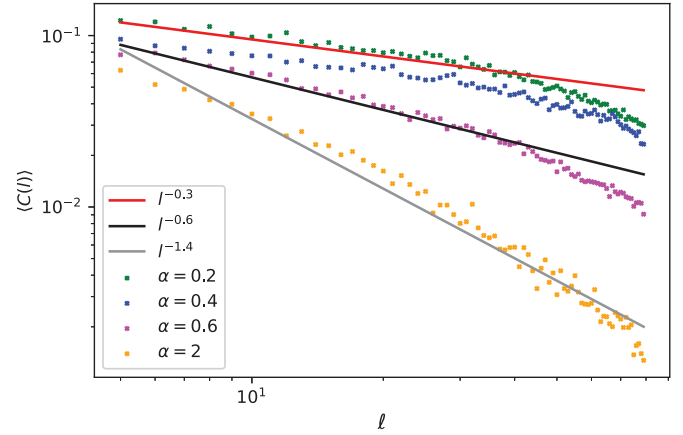


FIG. 14. Average correlation functions of excited eigenstates in the middle of the many-body spectrum as a function of the distance l as obtained via exact diagonalization for $N = 16$ spins. The filling factor $\frac{N}{L} = 0.1$ was considered for various values of α . The average was evaluated over 500 disorder realizations and $N_s = 50$ sampled states for each disorder realization.

is observed for $\alpha > \alpha^*$. We find that in the middle of the many-body spectrum, $\alpha^* \approx 1$ coincides with the delocalization transition α_c , which we derived from the level-spacing statistics obtained with ED for system sizes up to $N \sim 18$ spins to be at $\alpha_c \approx 1$ in the middle of the spectrum.

Using RSRG-X, we also investigate the entanglement contour for different values of α and find it to decay as a power of subsystem size l with power γ . We find good agreement for the conjecture that $\gamma \approx \alpha$. In an effort to derive this conjecture, we suggest a scaling theory based on the RG-rules structure for $\alpha \ll 1$. To illustrate and support this approach, we show typical eigenstate configurations as obtained with RSRG-X for $\alpha = 0.1$ and $\alpha = 1.6$.

In addition, we compute the half-chain EE at energy densities, which corresponds to a position away from the middle of the many body spectrum, and implement RSRG-X at lower effective temperature $T = 0.5$, corresponding to smaller energy density. The results indicate a crossover between a phase with strongly enhanced entanglement for $\alpha < \alpha^* \approx 0.6$ and a regime with logarithmic scaling of EE for $\alpha > \alpha^* \approx 0.6$. Thus, we find indications that $\alpha^* \leq \alpha_c$. This observation is consistent with the fact that in Ref. [26] we found in the ground state of the LR AFM coupled disordered spin chain that the area-law violation of EE is logarithmic for all α , so $\alpha^* \rightarrow 0$, while we had found previously that the delocalization transition in its ground state occurs at $\alpha_c \approx 1$ [24,25]. In summary, these results indicate that for $\alpha > \alpha_c$, the model behaves similarly as the nearest-neighbor random bond model [28], which was found to be in a quantum critical glass phase [9], a regime where arbitrarily high energy excited states exhibit power-law decaying correlation functions and logarithmic divergence in EE.

As excited eigenstates are states that participate in the dynamics of the system, understanding their properties is crucial to characterize quantum phase transitions. Therefore, building on these results for the higher energy eigenstates, we can

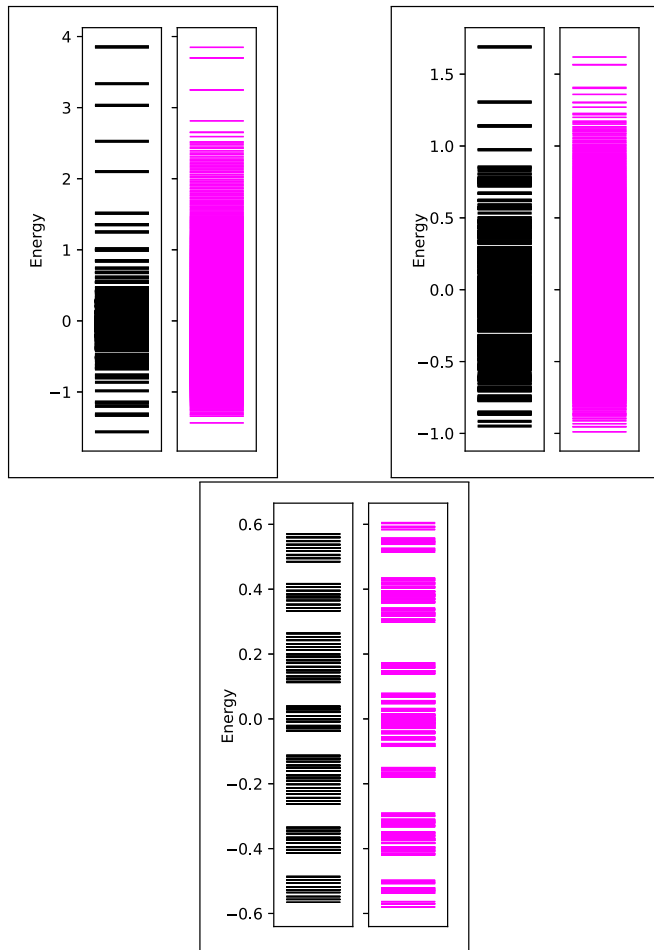


FIG. 15. Energy spectrums as obtained via RSRG-X (black) and ED (magenta) of the LR random spin chain. Results are obtained for $N = 10$, $L = 100$ with averaging over $M = 500$ disorder realizations, and for $\alpha = 0.4$ (top left), $\alpha = 0.8$ (top right) and $\alpha = 2$ (bottom).

aim in future research to study quantum quench dynamics in random spin chains with power-law LR couplings.

ACKNOWLEDGMENTS

We gratefully acknowledge the support from Deutsche Forschungsgemeinschaft (DFG) No. KE-807/22-1.

APPENDIX A: CORRELATION FUNCTIONS

Using numerical ED, we compute the mean correlation function between two spins at distance l . We sample N_s eigen-

states $|\psi_i\rangle$ in the middle of the many-body spectrum and compute the correlation function of spin i with another spin at distance l , $C_i(l)$:

$$C_i(l) = \frac{1}{N_s} \sum_{i=1}^{N_s} |\langle \psi_i | \sigma_i^y \sigma_{i+l}^y | \psi_i \rangle|. \quad (\text{A1})$$

Given a disorder realization, we then take the average of the correlation functions on different pairs of spins at the same distance l , yielding $C(l)$.

For a random singlet phase, it can be shown that the mean correlation function is proportional to the probability distribution of singlet lengths and thus decays as $C(l) \sim l^{-\eta}$ with $\eta = 2$ [38]. A similar result has been obtained via SDRG for the ground state of the LR random spin chain [26], while ED applied to the same model yielded $\eta \sim 1.4$ for small system sizes, independent of the value of the exponent α . For the rainbow chain, since all (odd) bond lengths are equiprobable one has that $\eta = 0$.

For excited eigenstates of the LR random spin chain, results for the average spin-spin correlation function are shown in Fig. 14. We see that the correlation functions decay with distance l as a power with an exponent η , $C(l) \sim l^{-\eta}$.

We find that the exponent η decays significantly for decreasing values of α . For $\alpha = 2$, η is close to what was found for the ground state of the same model [26], while decreasing α leads to smaller values for the exponent η , we find that $\eta \sim 0.3$ for $\alpha = 0.2$, approaching the result for the rainbow chain. These results support the rainbow-dimer coexistence picture for $\alpha \leq 1$, as η tends to 0 when α is decreased.

APPENDIX B: ENERGY SPECTRUM

To compare ED and RSRG-X, we have also considered the energy spectrums as obtained by the two methods for different values of α . Results are shown in Fig. 15. For the nearest-neighbor XX model with off-diagonal disorder, the chiral symmetry enforces a symmetric energy spectrum, while here it remains highly asymmetric. For $\alpha \gg 1$, the energy spectrum tends to become symmetric around $E = 0$, as for the nearest-neighbor chain. The two methods are in good qualitative agreement for the considered values of α , as can be observed in Fig. 15. We see that the energy bandwidths are comparable and of the same order for the considered values of α , eigenstate energy gaps are also comparable, and the same asymmetry with respect to $E = 0$ is observed for the two methods for the considered system size $N = 10$.

- [1] G. Feher, R. Fletcher, and E. Gere, *Phys. Rev. B* **100**, 1784 (1955).
- [2] P. W. Anderson, *Phys. Rev.* **109**, 1492 (1958).
- [3] L. Fleishman and P. W. Anderson, *Phys. Rev. B* **21**, 2366 (1980).
- [4] I. V. Gornyi, A. D. Mirlin, and D. G. Polyakov, *Phys. Rev. Lett.* **95**, 206603 (2005).

- [5] D. Basko, I. Aleiner, and B. Altshuler, *Ann. Phys.* **321**, 1126 (2006).
- [6] D. A. Abanin, E. Altman, I. Bloch, and M. Serbyn, *Rev. Mod. Phys.* **91**, 021001 (2019).
- [7] R. Bhatt and S. Kettmann, *Ann. Phys.* **435**, 168664 (2021).
- [8] J. M. Deutsch, *Phys. Rev. A* **43**, 2046 (1991).

- [9] R. Vasseur, A. Potter, and S. Parameswaran, *Phys. Rev. Lett.* **114**, 217201 (2015).
- [10] R. Vasseur, A. J. Friedman, S. A. Parameswaran, and A. C. Potter, *Phys. Rev. B* **93**, 134207 (2016).
- [11] D. J. Luitz, N. Laflorencie, and F. Alet, *Phys. Rev. B* **91**, 081103(R) (2015).
- [12] S. Schiffer, J. Wang, X.-J. Liu, and H. Hu, *Phys. Rev. A* **100**, 063619 (2019).
- [13] A. L. Burin, *Phys. Rev. B* **91**, 094202 (2015).
- [14] A. Safavi-Naini, M. L. Wall, O. L. Acevedo, A. M. Rey, and R. M. Nandkishore, *Phys. Rev. A* **99**, 033610 (2019).
- [15] C. Dasgupta and S.-k. Ma, *Phys. Rev. B* **22**, 1305 (1980).
- [16] F. Iglói and C. Monthus, *Phys. Rep.* **412**, 277 (2005).
- [17] G. Refael and J. E. Moore, *Phys. Rev. Lett.* **93**, 260602 (2004).
- [18] D. S. Fisher, *Phys. Rev. B* **50**, 3799 (1994).
- [19] E. Yusuf and K. Yang, *Phys. Rev. B* **68**, 024425 (2003).
- [20] C. A. Lamas, D. C. Cabra, M. D. Grynberg, and G. L. Rossini, *Phys. Rev. B* **74**, 224435 (2006).
- [21] R. Mélin, Y.-C. Lin, P. Lajkó, H. Rieger, and F. Iglói, *Phys. Rev. B* **65**, 104415 (2002).
- [22] J. A. Hoyos and E. Miranda, *Phys. Rev. B* **69**, 214411 (2004).
- [23] R. Juhász, I. A. Kovács, and F. Iglói, *Europhys. Lett.* **107**, 47008 (2014).
- [24] N. Moure, S. Haas, and S. Kettemann, *Europhys. Lett.* **111**, 27003 (2015).
- [25] N. Moure, H.-Y. Lee, S. Haas, R. N. Bhatt, and S. Kettemann, *Phys. Rev. B* **97**, 014206 (2018).
- [26] Y. Mohdeb, J. Vahedi, N. Moure, A. Roshani, H.-Y. Lee, R. N. Bhatt, S. Kettemann, and S. Haas, *Phys. Rev. B* **102**, 214201 (2020).
- [27] D. Pekker, G. Refael, E. Altman, E. Demler, and V. Oganesyan, *Phys. Rev. X* **4**, 011052 (2014).
- [28] Y. Huang and J. E. Moore, *Phys. Rev. B* **90**, 220202(R) (2014).
- [29] M. Pouranvari and K. Yang, *Phys. Rev. B* **92**, 245134 (2015).
- [30] P. Calabrese and J. Cardy, *J. Stat. Mech.: Theory Exp.* (2004) P06002.
- [31] C. Holzhey, F. Larsen, and F. Wilczek, *Nucl. Phys. B* **424**, 443 (1994).
- [32] G. Vidal, J. I. Latorre, E. Rico, and A. Kitaev, *Phys. Rev. Lett.* **90**, 227902 (2003).
- [33] H. Lipkin, N. Meshkov, and A. Glick, *Nucl. Phys.* **62**, 188 (1965).
- [34] R. G. Unanyan, C. Ionescu, and M. Fleischhauer, *Phys. Rev. A* **72**, 022326 (2005).
- [35] V. Oganesyan and D. A. Huse, *Phys. Rev. B* **75**, 155111 (2007).
- [36] A. Pal and D. A. Huse, *Phys. Rev. B* **82**, 174411 (2010).
- [37] A. Gubin and L. F. Santos, *Am. J. Phys.* **80**, 246 (2012).
- [38] J. A. Hoyos, A. P. Vieira, N. Laflorencie, and E. Miranda, *Phys. Rev. B* **76**, 174425 (2007).
- [39] S. Bravyi, D. P. DiVincenzo, and D. Loss, *Ann. Phys.* **326**, 2793 (2011).
- [40] A. D. Mirlin and F. Evers, *Phys. Rev. B* **62**, 7920 (2000).
- [41] M. Pouranvari and K. Yang, *Phys. Rev. B* **89**, 115104 (2014).
- [42] N. Roy, A. Sharma, and R. Mukherjee, *Phys. Rev. A* **99**, 052342 (2019).
- [43] G. Gori, S. Paganelli, A. Sharma, P. Sodano, and A. Trombettoni, *Phys. Rev. B* **91**, 245138 (2015).
- [44] J. Vahedi, A. Ashouri, and S. Mahdaviifar, *Chaos* **26**, 103106 (2016).
- [45] A. Ashouri, S. Mahdaviifar, G. Misguich, and J. Vahedi, *Annalen der Physik* **532**, 1900515 (2020).
- [46] Y. Chen and G. Vidal, *J. Stat. Mech.: Theory Exp.* (2014) P10011.
- [47] N. Samos Sáenz de Buruaga, S. N. Santalla, J. Rodríguez-Laguna, and G. Sierra, *Phys. Rev. B* **101**, 205121 (2020).
- [48] G. Vitagliano, A. Riera, and J. I. Latorre, *New J. Phys.* **12**, 113049 (2010).
- [49] G. Ramírez, J. Rodríguez-Laguna, and G. Sierra, *J. Stat. Mech.: Theory Exp.* (2014) P10004.
- [50] J. Rodríguez-Laguna, J. Dubail, G. Ramírez, P. Calabrese, and G. Sierra, *J. Phys. A: Math. Theor.* **50**, 164001 (2017).
- [51] V. Alba, S. N. Santalla, P. Ruggiero, J. Rodríguez-Laguna, P. Calabrese, and G. Sierra, *J. Stat. Mech.: Theory Exp.* (2019) 023105.